JOURNAL OF Materials CHEMISTRY

Electronic instabilities in lithium intercalated $ZrSe_2$

Claudia Felser,[a] Philippe Deniard,[b] Michael Bäcker,[c] Thorsten Ohm,[d] Jean Rouxel[b] and Arndt Simon[c]

[a]*Institut für Anorganische und Analytische Chemie, Johannes Gutenberg-Universität Mainz, Becher Weg 24, 55099 Mainz, Germany*

[b]*Institut des Matériaux de Nantes, 2 rue de la Houssinière, BP 32229, 44322 Nantes Cedex 3, France*

[c]*Max-Planck-Institut für Festkörperforschung, Heisenbergstr. 1, 70569 Stuttgart, Germany*

[d]*CRTBT-CNRS, 25, Avenue des Martyrs, 38402 Grenoble Cedex 09, France*

We have followed the evolution of the superconducting T_c on intercalation of Li in $ZrSe_2$ by means of magnetization studies at very low temperatures. To interpret the electronic structure and instabilities, we present the results of extensive LMTO-ASA band structure calculations on $ZrSe_2$ and the idealized compound $LiZrSe_2$. The experimental results suggest a picture of phase segregation in the intercalated samples into regions where Li atoms are a part of the percolating cluster and regions where the Li are not. The electronic structure calculations help to understand the nature of the bonding in this system and in particular, the nature of instabilities on the Fermi surface in the intercalated compounds. In keeping with certain models for the occurrence of superconductivity in systems whose electronic structures combine localized and itinerant behaviour, the title compounds display regions of high and low dispersion in the Fermi surface. A comparison with the superconducting spinel $LiTi_2O_4$ is particularly fruitful.

Introduction

Lithium intercalation in lamellar transition metal dichalcogenides has been extensively studied by many groups.[1] An interesting fact is the observation of superconductivity connected with a semiconductor to metal transition induced by Li intercalation in $ZrSe_{1.95}$ to give the compounds $Li_xZrSe_{1.95}$ ($x>0.4$).[2–7] The host compound $ZrSe_y$ is itself metallic for $1.85<y<1.90$. In the present work we have considered only host compositions $ZrSe_y$ with y between 1.91 and 1.95. Due to high localization of the electrons around the intercalated lithium ions, this semiconductor to metal transition is linked to the percolation threshold in the triangular lattice of the available sites in the van der Waals gap (Fig. 1). Such simulations could be performed using Monte Carlo methods, taking into account the fact that no Se atom has more than two Li atoms as neighbors, in keeping with results of ^{77}Se NMR experiments. Details are presented in reference 1. Li–Li interactions in the 2D network are responsible for the lowering of the percolation threshold from 0.50 to 0.42, the former value being expected for a classical 2D lattice gas model, and the latter being determined by Monte Carlo methods. The transition has been followed by various experimental techniques.[2,5,6] $ZrSe_2$ has an optical gap of 1.2 eV[8] and crystallizes in the CdI_2 structure. The intercalation proceeds without any change of the hexagonal closed packing within the layers, the Li occupying the octahedral sites within the van der Waals gap throughout the whole composition range ($0<x<1$). In the metallic region, an NMR study of the ^{77}Se peak on a $Li_{0.51}ZrSe_{1.95}$ sample shows that the Lorentzian lineshapes observed at room temperature split into two peaks below 250 K. The shift between the two peaks is proportional to the applied magnetic field. This excludes any magnetic dipolar interaction between nuclei and suggests a modulation of the electron density induced by a screening effect, due to the potential of Li^+ ions. This lineshape is in good agreement with a computer simulation of a structure with alternating rows of empty and occupied lithium sites as seen in Fig. 2. In this figure, one can see that half the selenide ions have one lithium first neighbor and half of them have two lithium first neighbors. The ^{77}Se NMR experiments are thus a powerful tool for analysing the lithium distribution in these compounds.

We have investigated the electronic properties of different superconducting systems such as $Y_2Br_2C_2$,[9–11] $La_6Br_5(BC_2)_3$,[12] YC_2,[13] Hg,[14] compounds with the $ThCr_2Si_2$ structure type such as $LuNi_2B_2C$,[15] La_3S_4,[16] $LiTi_2O_4$,[17] $ZrTe_3$[18] and $La_2CaCu_2O_6$[19] in order to extract the chemical features that could be important for superconductivity. For chemists, directives on how to prepare new superconductors are few. Momentum space explanations such as the two band model[20] and the van Hove scenario[21,22] have to be translated into a

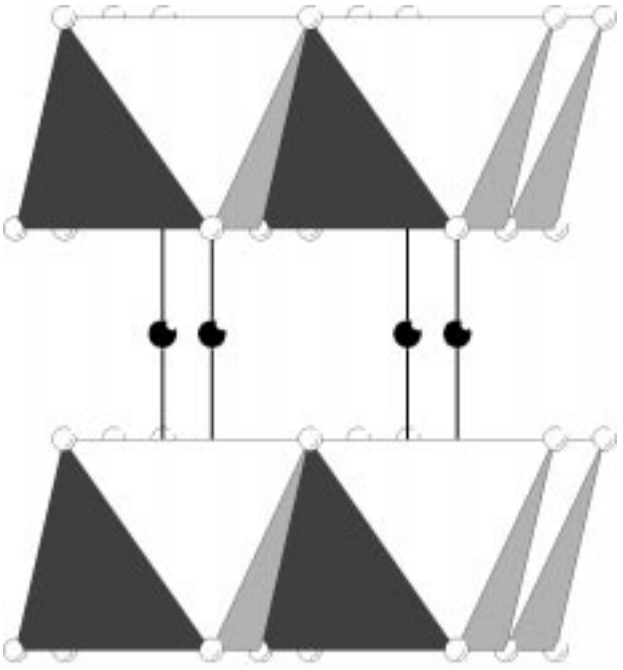

Fig. 1 Crystal structure of $LiZrSe_2$. The Zr occupy the centers of Se_6 octahedra. The Li atoms are black and occupy octahedral voids between the sheets of octahedra.

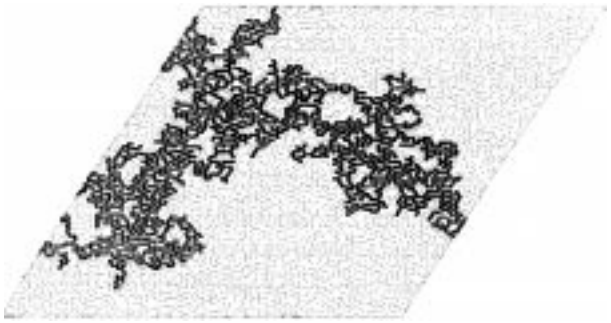

Fig. 2 A computer simulation of the percolation model for $Li_{0.42}ZrSe_{1.95}$. The simulation uses the fact that no Se atom has more than 2 Li neighbors so that percolation takes place at $x=0.42$ rather than $x=0.5$ expected on a triangular lattice without interactions. The percolating cluster at the percolation threshold is displayed using bold points. The points are Li atoms that do not make up a part of this cluster.

real space picture for chemical applications. Our systematic investigations of the electronic properties of many compounds have rendered the possibility of extracting some important features in the band structures of these compounds that may have some bearing on the occurrence of superconductivity as well as on the transition temperature. The balance of electrons between localization and delocalization seems to be a necessary condition for superconductivity. In the momentum space description, this condition requires a band structure that has regions of both high and low dispersion in the vicinity of the Fermi energy. The regions of high dispersion or high Fermi velocity correspond to delocalization and the regions of low dispersion or low Fermi velocity correspond to localized states.[9]

Although T_c is low in Li intercalated $ZrSe_{1.95}$, from a theoretical point of view the system is interesting in order to isolate important features associated with superconductivity and to compare the electronic properties of this system with other systems. A comparison with the spinel superconductor $LiTi_2O_4$ is particularly fruitful.[23] T_c in this spinel is around 12 K and a metal to semiconductor transition is found by doping the conduction band with more than 0.33 holes per formula unit.

We have reinvestigated the magnetic properties of Li doped $ZrSe_2$ at low temperatures, especially the superconducting transition temperature as a function of the amount of intercalated Li. To connect our experimental results with some theoretical ideas we have performed TB-LMTO-ASA band structure calculations on the host compound and an idealized, fully intercalated $LiZrSe_2$.

Experimental details

$ZrSe_{1.95}$ was prepared by direct reaction of the elements in sealed silica tubes at 923 K after a preliminary heat treatment in two steps at 573 K and 773 K. Stoichiometry was determined by calcination. Intercalation of the host material was achieved using *n*-butyllithium in a glove box containing less than 1 ppm of both water and oxygen. Controlling the amounts of *n*-butyllithium allowed the Li content in the intercalated product to be varied. Following this, annealing of the intercalated material at 623 K for 4 days was performed for homogenization. Lithium content was determined by atomic absorption spectroscopy with a Philips PU9000 spectrometer. In addition to this sample characterization, we determined cell parameters by refinement of X-ray profiles of all the $Li_xZrSe_{1.95}$ compounds using the Prolix[24] and U-fit[25] programs, and FullProf[26] in full pattern matching mode. This helped to verify the structural homogeneity in relation to the Li composition since the cell parameters are very sensitive to lithium content in the metallic region.[27] An analysis of the linewidths of the different profiles could, after deconvolution of instrumental contributions, provide some information on homogeneity in the structure. Such an analysis is complicated for two reasons. The first is that the low temperatures of sample preparation yield very small crystallites and thus, rather broad linewidths in the X-ray profiles. Separation of the contributions to linewidth due to strain and size effects has proved difficult. Secondly, the undoped material is itself non-stoichiometric and thus the material could be strained even in the absence of intercalant atoms. For magnetic measurements, the intercalated samples ($x=0.33$, 0.66, 0.75 and 1) were placed in copper cylinders (4 mm diameter, 5 mm length) to protect them from moisture. The cylinder was sealed with Torr Seal epoxy resin. We performed the magnetization measurements using a dc SQUID magnetometer in the 100 mK–10 K temperature range. The raw data were corrected from paramagnetic behaviour due to additional materials present (*i.e.* Teflon tape, copper cylinder, glue *etc.*). To allow a comparision between the samples, the magnetization curves were scaled by the $Li_xZrSe_{1.95}$ sample mass.

Computation details

First principles self-consistent LDA[28] calculations of the electronic structure were performed using the LMTO-ASA method. A detailed description of the LMTO-ASA method, including its application to the electronic structure of compounds, has been given elsewhere[29,30] and only selected details are provided here. The scalar relativistic Kohn–Sham–Schrödinger equations were solved taking all relativistic effects into account except for the spin–orbit coupling. All *k*-space integrations are performed with the tetrahedron method using 213 irreducible *k*-points within the Brillouin zone (BZ). The BZ is as described in ref. 31, where the symmetry points and lines are labelled in accordance with the standard notation. The band structure was calculated for the Bloch vectors along the following lines: Γ (0,0,0) to K (2/3,1/3,0) to M (1/2,0,0) to Γ and from A (0,0,1/2) to L (1/2,0,1/2) to H (2/3,1/3,1/2) to Γ in units of ($2\pi/a$, $2\pi/a$, $2\pi/c$). The basis set consisted of s, p and d orbitals for Zr, s and p orbitals for Se and s for Li. The positions and radii of the empty spheres were calculated using an automatic procedure developed by Krier *et al.*[32] The lattice constants from Table 1 and the idealized symmetry were utilized. Defects in the host structure were neglected and only the band structures of the host and of the fully intercalated compound were calculated. To investigate the bonding situation at the Fermi level, two new tools of the program package of Andersen *et al.* were used. Within the so called fatband representation,[33] the orbital character of each band can be easily demonstrated by decorating specific bands with a width that is proportional to the sum of the weights of the corresponding orthonormal orbitals. The use of COHPs (crystal orbital Hamiltonian population)[34] helps to decide whether an orbital interaction is bonding or antibonding. The COHP diagram is similar to the COOPs introduced by Hoffmann and coworkers,[35] marking bonding, nonbonding or antibonding energy regions of specific atomic orbitals.

Magnetic measurements

Fig. 3 details the magnetic studies on the intercalated samples, showing the superconducting transition. As expected from the

Table 1 Structures of $ZrSe_2$ and $LiZrSe_2$ (space group: $P\bar{3}m1$)

	atom	*x*	*y*	*z*
$ZrSe_2$: $a=3.7688$ Å	Zr	0	0	0
$c=6.1400$ Å	Se	−1/3	1/3	−0.2500
$LiZrSe_2$: $a=3.7340$ Å	Li	0	0	1/2
$c=6.4800$ Å				

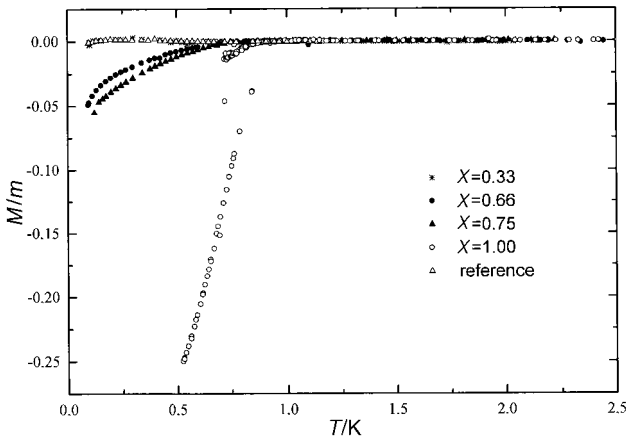

Fig. 3 Magnetization at low temperatures for Li_xZrSe_2 (x indicated in figure). The magnetization (in emu) has been scaled by the sample mass.

previous studies, $Li_{0.33}ZrSe_{1.95}$[7] is the only sample of those studied that does not present diamagnetic behaviour at low temperatures. In fact, at this composition, the intercalated compound is still below the percolation threshold for the lithium ions on the triangular lattice of the available sites for lithium intercalation and, hence, has semiconducting behaviour at high temperature. The large ion–electron interaction at this stage can then be considered as responsible for an Anderson localization of the electrons given up by the lithium atoms. The same effect has been observed in $LiTi_2O_4$.[23] In this compound also, hole doping over a certain threshold leads to semiconducting behaviour that is correlated with the destruction of superconductivity. In both compounds, superconductivity can be observed between 1 and *ca.* 0.6 electrons per formula unit in the conduction band.

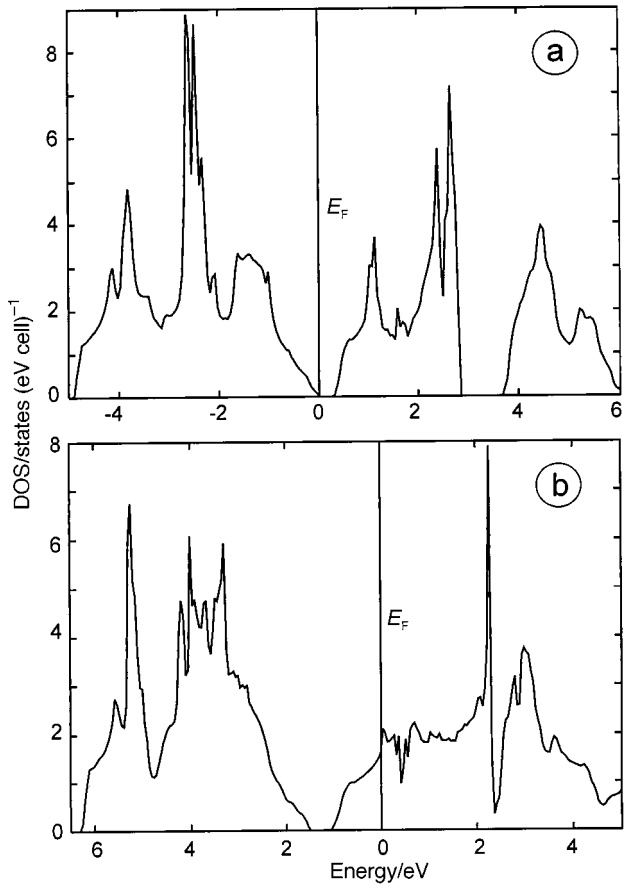

Fig. 4 Total LMTO-ASA density of states for (a) $ZrSe_2$ and (b) $LiZrSe_2$. The vertical lines depict the Fermi energy.

For $Li_xZrSe_{1.95}$ with $x=0.66$, 0.75 and 1.00, a superconducting transition is observed. The transition is sharp for $x=1.00$ with a T_c (onset) of 0.8 K. For $x=0.66$ and $x=0.75$ the transition is less sharp and the onset temperature is slighly lower. This observation agrees again with the behaviour of the superconducting transition of the different hole doped spinel samples. The T_c trend as function of the number of doped electrons observed in Li_xZrSe_2 and in $LiTi_2O_4$ as well is difficult to rationalize in terms of the BCS theory or in terms of the van Hove scenario. We expect a rapid drop of T_c as $N(E_F)$ drops with decreasing Li content. A variation of T_c with changing $N(E_F)$ would be anticipated in sharp contrast to the observed persistence of T_c across a range of x. In the absence of a satisfactory explanation for the T_c behaviour, microscopic chemical inhomogeneities have to be considered. An investigation of the superconducting volume fraction *vs.* content can show whether phase separation as discussed in connection with the high T_c cuprates and $LiTi_2O_4$[36] is a possible explanation. Unfortunately, we are unable to do so with the present samples, whose form (powders) and air sensitivity (requiring encapsulation in Cu cylinders) makes volume fraction determinations unreliable. Our observations are however consistent with the idea that with increasing Li content, there are regions of the sample that have Li as a part of the percolating cluster and are superconducting, and regions of the sample where Li are not a part of the percolating cluster. These are insulating. This is related to the percolation of Li at $x=0.42$ that gives rise to the composition dependent localized to extended transition in the first place.

Electronic properties

Density of states and energy bands

As an overview over the electronic properties of $ZrSe_2$ and $LiZrSe_2$, the total densities of states $N(E)$ are shown in Fig. 4(a)

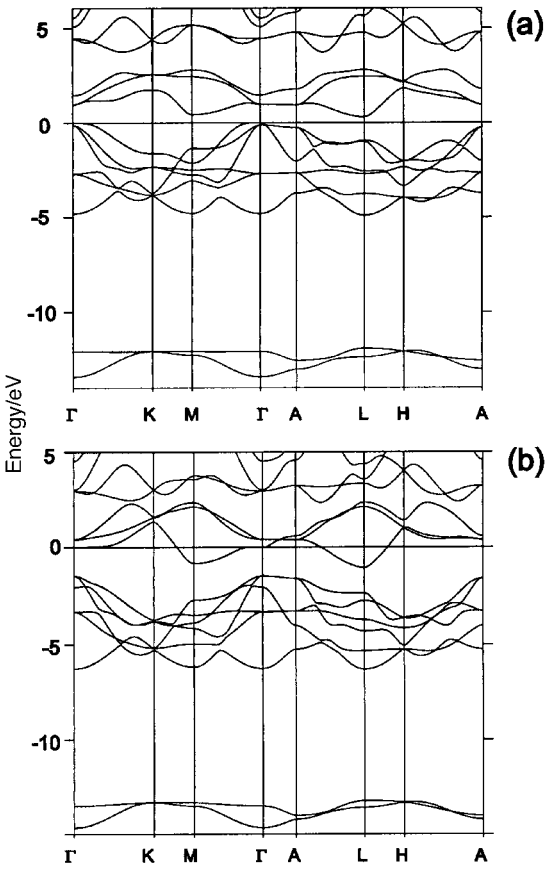

Fig. 5 Band structures of (a) $ZrSe_2$ and (b) $LiZrSe_2$

and (b). As expected from the optical measurements, a gap of 0.5 eV at E_F is found for the host compound $ZrSe_2$. Compared with the experimental value of 1.2 eV, the calculated gap is small. It is well established that within the LDA calculated gaps are always smaller than the experimental ones. The states below E_F have mainly Se p character and are shown in Fig. 4(a) between -5 eV and the Fermi energy. Nearly all Zr d states are empty (d^0). Due to the octahedral crystal field, the Zr d block splits up into three t_{2g} (d_{xy}, d_{xz}, d_{yz}) and two e_g (d_{z^2}, $d_{x^2-y^2}$) orbitals. There might be a substantial metal–metal interaction, because of the edge-shared octahedra, as reflected in broad t_{2g} levels between 0.4 and 3 eV. Between the t_{2g} and the e_g levels in $ZrSe_2$, there is a gap of 1 eV. In Fig. 4(b) the total DOS of fully intercalated $LiZrSe_2$ is shown. The states at the Fermi level have mainly Zr d character with a small contribution from Se p states. Because of the ionic character of lithium we expect only a shifting of the position of the Fermi level through doping. This would be in agreement with a rigid band model under the assumption of total charge transfer of one electron from the Li to the $ZrSe_2$ layers. The Fermi level coincides nearly with a peak in the density of states, which indicates a three dimensional van Hove singularity. The width of the Se p states is the same as found for the band structure of the host compound, but the t_{2g} levels of $LiZrSe_2$ are slightly broader (3.5 eV *vs.* 2.5 eV). The width and the position of the Zr e_g levels relative to the Se p states have not changed. Therefore the gap between the t_{2g} and the e_g levels is closed. Between Se and Zr states there is a gap of 0.5 eV.

Bands structure and Fermi surface

The band structures of $ZrSe_2$ and $LiZrSe_2$ are shown in Fig. 5(a) and (b) respectively. There is an indirect gap of 0.5 eV between Γ and L. From the view point of the band structure, the compound is not really two dimensional, the dispersion especially of the six selenium p bands (between -5 eV and the Fermi energy) perpendicular to the layers (Γ–A) is high. The t_{2g} bands between 0.5 eV and 3 eV are well separated from the two e_g bands around 4.5 eV above E_F. Also the highest lying t_{2g} band shows some dispersion along Γ–A.

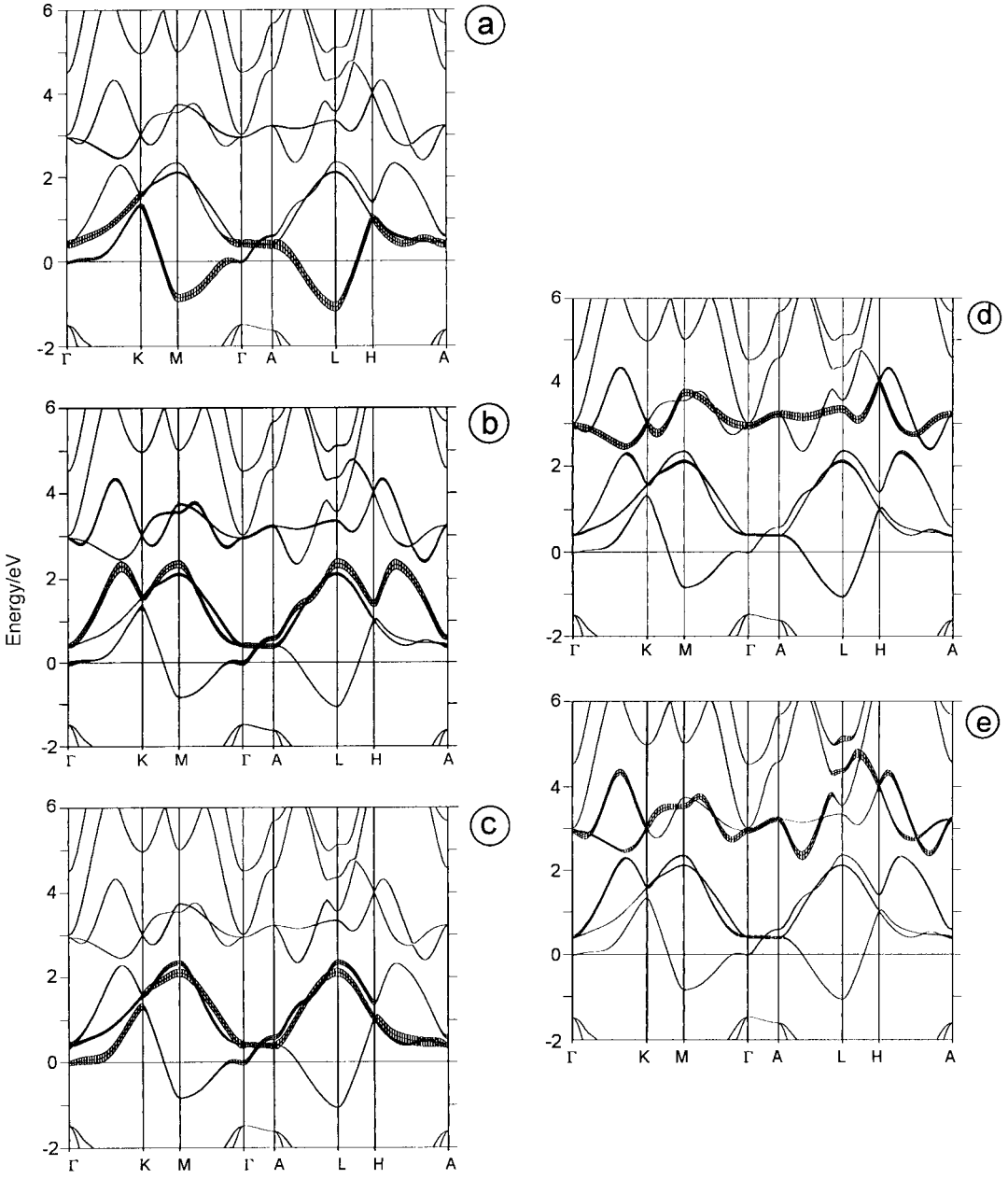

Fig. 6 Fatband representations for $LiZrSe_2$. A width of 0.2 eV (2.5% of the total energy scale) represents the 'pure' 100% orbital contribution. The fatbands are for (a) Zr d_{xy}. (b) Zr d_{xz}, (c) Zr d_{yz}, (d) Zr $d_{x^2-y^2}$ and (e) Zr d_{z^2}.

Closer examination of the overall band structure of $ZrSe_2$ compared with the lithium intercalated compound shows that the rigid band model is no longer valid. The effect of lithium intercalation is not merely electron donation, influences the band structure in these compounds as well, especially the character of the bands around E_F. Whereas the top of the valence band of $ZrSe_2$ at the Γ point has π character, this band for $LiZrSe_2$ is degenerate with Se p_x, p_y and Zr e_g eigenvector contributions (σ interaction). The opposite situation is found for the lowest lying band of the conduction band at the Γ point. In the lithium intercalated compound the nondegenerate band, with dispersion also in the Γ–A direction, crosses the Fermi level and builds up the Fermi surface. The cause of the change in the ordering of the bands is not the Li atom itself but rather the drastic change of the *c* lattice parameter. The calculation on $ZrSe_2$ with the lattice constants of the fully intercalated compound, but without Li atoms in the van Waals gap, leads to the same ordering of bands as we find for $LiZrSe_2$.

The band structure of lithium intercalated $ZrSe_2$ in the fatband representation is seen in Fig. 6(a)–(e). There are two different ways to describe the bonding situation in this structure type. If we set the *z* axis equal to the crystallographic *c* axis, it is difficult to demonstrate the octahedral crystal field splitting. Therefore we transform the orbitals to the internal coordinates of the octahedron. We are mainly interested in the bonding situation around E_F which is the cause of the exceptional properties. Therefore only the fatbands of the Zr d orbital are shown. Not shown in the fatband representation in Fig. 6 are two Se s bands situated at −14.7 eV and −13.5 eV (energies at Γ). Within the internal coordinate system a classification of σ and π bonding interaction is possible. The selenium p_z band with a small contribution from the t_{2g} levels is found at −6.2 eV (π interaction). At the Γ point two degenerate σ bands, which have Se p_x, p_y and e_g character contribute to the band at −3.3 eV. At −2.1 eV there is again a π type interaction, and the top of the valence band is derived from degenerate σ bonds with mainly selenium character. As expected from the atomic orbital energies, the Zr contribution to the bands increases with the energy. The conduction band, shown in Fig. 6(a)–(c), crosses E_F and is built by the Zr t_{2g} levels. Only the selenium p_z orbital contributes to these three bands. The bottom of the conduction band has mainly Zr d_{xy} character, only along the Γ–A direction do the d_{xz} and d_{yz} contributions dominate. The degradation of this band relative to the degenerate t_{2g} bands of $ZrSe_2$ is influenced by the increase of the *c*-axis. Within the crystallographic coordination system this small saddle point at Γ has only d_{z^2} character, a hint that the interaction perpendicular to the planes plays an important role. At the Γ point 2.95 eV above the Fermi energy the degenerate e_g bands are found. The selenium–zirconium interaction of these bands has σ character. Because of this, the fatbands have only Se p_x and p_y contributions. A few meV above, the highly dispersive lithium s band is seen.

The Fermi surface of $LiZrSe_2$ is shown in Fig. 7. The representation projects down c^* perpendicular to the plane which contains Γ, M and K parallel to the Γ–A direction. The colours of the plot reflect the Fermi velocity, where red means a high Fermi velocity and blue low Fermi velocity. From the band structure we know that only one nondegenerate half-filled band crosses E_F. Therefore there is only one envelope of the Fermi surface. From a first impression, the Fermi surfaces reflect nicely the hexagonal symmetry, and the system seems to be two dimensional. There is however a small blue square at the zone center that is parallel to the c^* direction. The so called van Hove singularity, associated with a saddle point, is three dimensional as known from the band structure and is responsible for the three dimensional Fermi surface. Around Γ there is a region of holes and along Γ–M a relatively flat band crosses E_F. Electrons are around M and L. In agreement with certain models which discuss the balance of carriers between localization and delocalization as a condition for superconductivity, this Fermi surface has localized (blue) and delocalized (red) regions.

Bonding situation

The dominant bonding interaction in $ZrSe_2$ is surely the zirconium–selenium interaction. Because of the charge transfer of four electrons from zirconium to the selenium atoms we expected no Se–Se or Zr–Zr bond in this structure type. On the other hand the edge shared octahedra render possible a metal–metal interaction. The metal–metal distance (3.77 Å) is much larger compared with the spinel type compound, where the metal–metal bond plays an important role. To clarify this question, we calculated the COHPs for the Zr–Se, Zr–Zr and Se–Se interaction as seen in Fig. 8(a)–(e). The Zr–Se interaction is the strongest interaction as expected, bonding below E_F

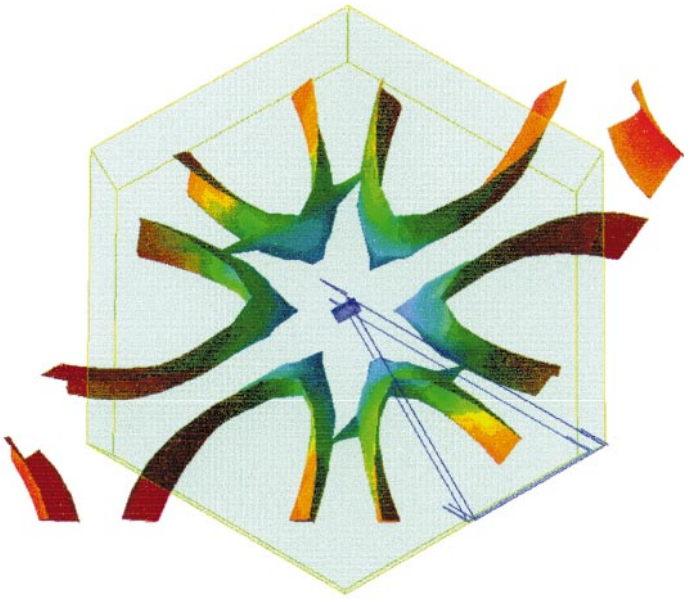

Fig. 7 LMTO-ASA Fermi surface of $LiZrSe_2$. Red regions correspond to high dispersion (high Fermi velocity) and blue regions to fat bands (low Fermi velocity).

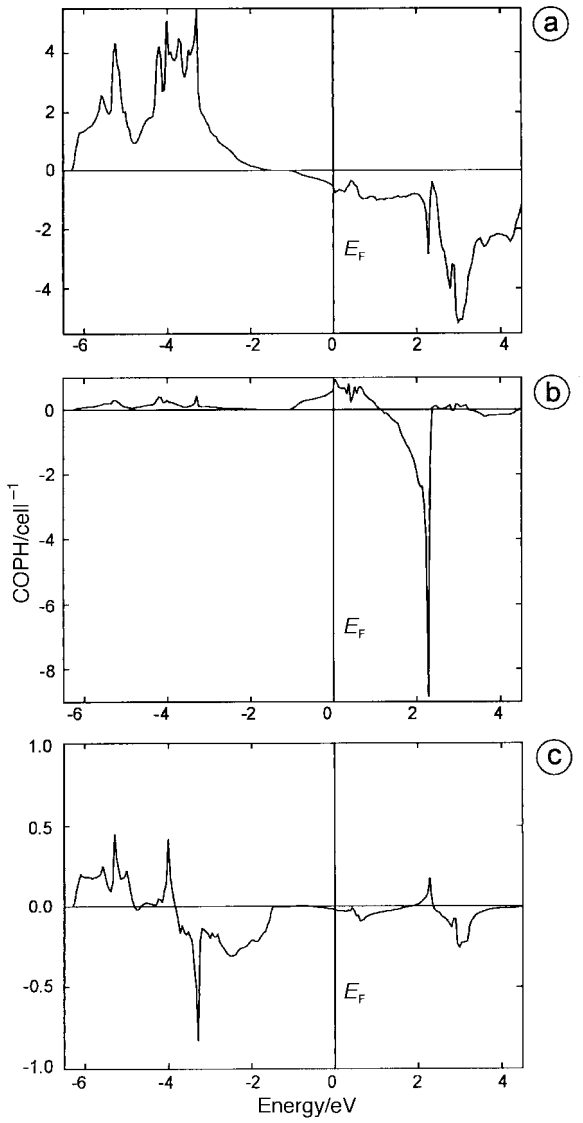

Fig. 8 COHPs of $LiZrSe_2$: (a) Zr—Se (b) Zr—Zr and (c) Se—Se. Positive values indicate bonding interactions and negative antibonding.

where the Se states dominate the DOS and antibonding at E_F and above. As we know from our fatband representation, the contribution to the states at E_F comes from the metal t_{2g} orbitals and therefore has π character. Much stronger, though not interesting for the physical properties, are the σ-type Se p–Zr e_g interactions between 2 and 4 eV above E_F. The metal–metal interaction starts as expected around E_F at the bottom of the conduction band and becomes antibonding at the top of the t_{2g} band. A small Se–Se bonding interaction has to be recognized below E_F due to charge transfer back from Se to Zr. Qualitatively and quantitatively we find here the same bonding situation as in the spinel type compound $LiTi_2O_4$. The additional electron from Li occupies a band which is bonding due to the Ti–Ti (here Zr–Zr) interaction and antibonding due to the Ti–O (Zr–Se) interaction. The strength of the bonding as determined from the magnitude of the COHP is also very similar for the two systems.

Conclusion

From the viewpoint of band structure, $LiZrSe_2$ can be compared with the cubic superconductor $LiTi_2O_4$. Both compounds are d^1 systems (referring to one formula unit), and in both compounds a metal to semiconductor transition takes place when the t_{2g} band filling is less than 0.33 electrons per transition metal atom. Connected with the metal to semiconductor transition, superconductivity occurs in both compounds. The transition temperature does not depend upon the composition and therefore an explanation within BCS theory is not possible. The peculiar T_c trend investigated for $Li_xZrSe_{1.95}$ in this paper and also observed for hole doped $LiTi_2O_4$[36] can be explained on the basis of a percolation model. Bonding metal–metal (Zr–Zr) interactions play the dominant role at E_F. Antibonding Zr–Se interactions are important but the number of Se states at or near E_F are small. Thus the intercalation of Li into $ZrSe_2$ results in both Zr and Se states being affected. From our band structure calulations, we find a small three-dimensional saddle point at E_F which coexists with some highly dispersive regions; this saddle point is at the Γ point which has high symmetry and therefore low degeneracy. This may explain why T_c in this system is so low compared with, for example, the spinel.

We thank E. Rocholz for help with preparing the plots. O. K. Andersen, O. Jepsen and F. Boucher are thanked for providing the LMTO code and for support and encouragement. This work was supported by the Deutsche Forschungsgemeinschaft and the region des Pays de Loire, France.

References

1 R. Brec, P. Deniard and J. Rouxel, in *Progress in intercalation research*, ed. W. Müller-Warmuth and R. Schöllhorn, Kluwer, Amsterdam, 1994, pp. 177–221; *Intercalation in layered materials*, ed. M. S. Dresselhaus, NATO Advanced Series B148, Plenum, New York, 1987 and references therein.
2 Y. Onuki, T. Hirai, K. Shibutami and T. Komatsubara, *J. Inclusion Phenom.*, 1984, **2**, 279.
3 Y. Onuki, R. Inada, S. Tanuma, S. Yamanaka and H. Kamimura, *J. Phys. Soc. Jpn.*, 1982, **51**, 880; *Synth. Met.*, 1983, **5**, 245.
4 P. Deniard, P. Chevalier, L. Trichet, Y. Chabre and J. Pannetier, *Solid State Commun.*, 1987, **64**, 175.
5 C. Berthier, Y. Chabre, P. Segransan, P. Chevalier, L. Trichet and A. Lé Méhauté, *Solid State Ionics*, 1981, **5**, 379.
6 C. Berthier, Y. Chabre, P. Segransan, P. Deniard, L. Trichet and J. Rouxel, *Physics and chemistry of electrons and ions in condensed matter*, ed. J. V. Acrivos, N. F. Mott and A. D. Yoffe, NATO Advanced Series C130, Riedel, Dordrecht, 1985, p. 561.
7 D. W. Murphy, F. J. Di Salvo, G. W. Hull, Jr. and J. V. Waszcak, *Inorg. Chem.*, 1976, **15**, 17.
8 J. von Boehm and H. M. Isomaki, *J. Phys. C: Solid State Phys.*, 1982, **15**, L733.
9 A. Simon, A. Yoshiasa, M. Bäcker, R. W. Henn, C. Felser, R. K. Kremer and H. Mattausch, *Z. Anorg. Allg. Chem.*, 1996, **622**, 123; A. Simon, *Angew. Chem.*, 1997, **109**, 1873; *Angew. Chem., Int. Ed. Engl.*, 1997, **36**, 1789.
10 A. Schwanitz-Schüller and A. Simon, *Z. Naturforsch.*, 1985, **407**, 10.
11 R. W. Henn, W. Schnelle, R. K. Kremer and A. Simon, *Phys. Rev. Lett.*, 1996, **77**, 374.
12 H. J. Mattausch, A. Simon, C. Felser and R. Dronskowski, *Angew. Chem.*, 1996, **108**, 1805; *Angew. Chem., Int. Ed. Engl.*, 1996, 1685.
13 T. Gulden, R. W. Henn, O. Jepsen, R. K. Kremer, W. Schnelle, A. Simon and C. Felser, *Phys. Rev. B*, 1997, **56**, 9021.
14 S. Deng, A. Simon and J. Köhler, *Angew. Chem.*, 1998, **110**. 664.
15 D. Johrendt, C. Felser, O. Jepsen, O. K. Andersen, A. Mewis and J. Rouxel, *J. Solid State Chem.*, 1997, **130**, 254.
16 C. Felser, *J. Alloys Compd.*, 1997, **61**, 87.
17 C. Felser, in preparation.
18 W. Finckh, C. Felser and W. Tremel, *J. Alloys Compd.*, 1997, **61**, 97.
19 C. Felser, R. Seshadri, A. Leist and W. Tremel, *J. Mater. Chem.*, 1998, **8**, 789.
20 R. Micnas, J. Ranninger and S. Robaszkiewicz, *Rev. Mod. Phys.*, 1990, **62**, 113.
21 J. Labbé and J. Bok, *Europhys. Lett.*, 1987, **3**, 1225.
22 D. M. Newns, H. R. Krishnamurthy, P. C. Pattnaik, C. C. Tsuei, C. C. Chi and C. L. Kane, *Phys. B*, 1993, **186**, 801.
23 D. C. Johnston, H. Prakash, W. H. Zachariasen and R. Viswanathan, *Mater. Res. Bull.*, 1973, **8**, 777; D. C. Johnston, *J. Low Temp. Phys.*, 1976, **25**, 145.
24 P. Deniard, M. Evain, J. M. Barbet and R. Brec, *Mater. Sci. Forum.*, 1991, **363**, 79.

25 M. Evain, U-Fit manual, internal report of the IMN Nantes, France, 1992.
26 J. Rodriguez-Carvajal, *Physica B*, 1993, **192**, 55.
27 P. Deniard, P. Chevalier, L. Trichet and J. Rouxel, *Synth. Met*., 1983, **5**, 141.
28 U. von Barth and L. Hedin, *J. Phys. C*, 1972, **4**, 2064.
29 O. K. Andersen and O. Jepsen, *Phys. Rev. Lett*., 1984, **53**, 2571; O. K. Andersen, Z. Pawlowska and O. Jepsen, *Phys. Rev. B*, 1986, **34**, 5253.
30 H. L. Skriver, *The LMTO method*, Springer, Berlin, 1984.
31 C. J. Bradley and A. P. Cracknell, *The mathematical theory of symmetry in solids*, Clarendon Press, Oxford, 1972.
32 G. Krier, O. Jepsen and O. K. Andersen, unpublished results.
33 O. Jepsen and O. K. Andersen, *Z. Phys. B*, 1995, **97**, 35.
34 F. Boucher, O. Jepsen and O. K. Andersen, unpublished results.
35 S. D. Wijeyesekera and R. Hoffmann, *Organometallics*, 1984, **3**, 949; R. Hughbanks and R. Hoffmann, *J. Am. Chem. Soc*., 1983, **106**, 3528.
36 P. M. Lambert, P. P. Edwards and M. R. Harrison, *J. Solid State Chem*., 1990, **89**, 345.

Paper 7/08715B; *Received* 3*rd December*, 1997